ELSEVIER

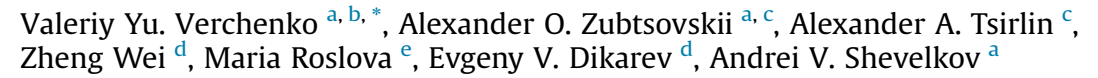
Contents lists available at ScienceDirect

Journal of Alloys and Compounds

journal homepage: http://www.elsevier.com/locate/jalcom



Mo₆Ga₃₁ endohedral cluster superconductor





^b National Institute of Chemical Physics and Biophysics, 12618, Tallinn, Estonia

ARTICLE INFO

Article history:
Received 27 May 2020
Received in revised form
10 July 2020
Accepted 13 July 2020
Available online 6 August 2020

Keywords: Superconductivity Strong coupling Intermetallic

ABSTRACT

Endohedral cluster compounds are a rich source of new superconductors, where nontrivial properties are expected, including strong coupling regime and multigap superconductivity. Here, we report on the synthesis, crystal and electronic structure, and physical properties of the Mo_6Ga_{31} endohedral cluster superconductor. The compound has two crystallographic modifications, monoclinic and triclinic, which are built by the $Mo@Ga_{10}$ endohedral clusters. Both structures possess qualitatively the same electronic density of states showing a high peak at the Fermi level. Due to the proximity effect of the triclinic and monoclinic domains, which are in the strong contact with each other, bulk Mo_6Ga_{31} exhibits single superconducting transition at the critical temperature of 8.2 K in zero magnetic field. The upper critical field, which is 7.8 T at zero temperature, shows clear enhancement with respect to the Werthamer-Helfand-Honenberg prediction. Accordingly, heat capacity measurements indicate strong electron-phonon coupling in the superconducting state with the large ratio of $2\Delta(0)/(k_BT_c)=4.5$, where $2\Delta(0)=3.2$ meV is the full superconducting gap at zero temperature.

© 2020 Elsevier B.V. All rights reserved.

- Mo₆Ga₃₁ intermetallic superconductor is composed of Mo@Ga₁₀ endohedral clusters, which form {Mo₁₂Ga₆₂} superprism building units.
- Bulk Mo₆Ga₃₁ inherently contains monoclinic and triclinic domains, where {Mo₁₂Ga₆₂} units are perpendicular or codirectional, respectively.
- Due to the proximity effect, Mo₆Ga₃₁ demonstrates single superconducting transition below the critical temperature of $T_c = 8.2$ K and upper critical field of $\mu_0 H_{c2} = 7.8$ T.
- Mo₆Ga₃₁ exhibits strong coupling superconductivity with the extremely large ratio of $2\Delta(0)/(k_BT_c) = 4.5$.

1. Introduction

Recently, the tra1nsition metal-embedded Ga clusters were proposed as a structural motif favorable for superconductivity [1].

E-mail address: valeriy.verchenko@gmail.com (V.Yu. Verchenko).

Endohedral Ga clusters centered by 4d or 5d transition metals can be found in the crystal structures of Ga-rich binary intermetallic compounds, among which ${\rm Mo_8Ga_{41}}$ with $T_c=9.8{\rm K}$ [2], ${\rm Mo_6Ga_{31}}$ (8 K) [3], ${\rm Mo_4Ga_{21-x-\delta}Sn_x}$ (5.85 K) [4], ${\rm ReGa_5}$ (2.3 K) [1], ${\rm Rh_2Ga_9}$ (1.9 K) [5], and ${\rm Ir_2Ga_9}$ (2.2 K) [5] exhibit superconducting properties. In this list, the Mo-based superconductors are distinguished by higher critical temperatures. A closer look reveals that they possess superconducting-state propeties deviating from the Bardeen-Cooper-Schriffer (BCS) model. (see Table 1)

For Mo_8Ga_{41} , measurements of heat capacity indicate strong coupling superconductivity with the full superconducting gap of $2\Delta(0)/(k_BT_c)=4.4$ exceeding significantly the weak-coupling BCS limit [6,7]. Furthermore, muon spin rotation/relaxation (μ SR) experiments show possible multigap or multiband superconductivity [8] that may originate from the site-selective mechanism involving two Fermi-surface sheets with different band velocities [9,10]. In the two independent studies, scanning tunneling spectroscopy was employed to directly probe the multigap behavior of Mo_8Ga_{41} . While measurements on polycrystalline samples confirmed the two-gap scenario [9], study of single crystals revealed the formation of surface domains, where spatially resolved single-gap order



c Experimental Physics VI, Center for Electronic Correlations and Magnetism, Institute of Physics, University of Augsburg, 86135 Augsburg, Germany

^d Department of Chemistry, University at Albany, SUNY, Albany, 12222, New York, United States

^e Department of Materials and Environmental Chemistry, Stockholm University, SE-106 91, Stockholm, Sweden

^{*} Corresponding author. Department of Chemistry, Lomonosov Moscow State University, 119991, Moscow, Russia.

Table 1 Normal- and superconducting-state parameters of the Mo₈Ga₄₁[6,7], Mo₆Ga₃₁, and Mo₄Ga_{21-x- δ}Sn_x[4] endohedral cluster superconductors; m refers to the monoclinic polymorph of Mo₆Ga₃₁, and t to triclinic.

Parameter	Mo ₈ Ga ₄₁	Mo ₆ Ga ₃₁	$Mo_4Ga_{21-x-\delta}Sn_x$
T_c (K)	9.8	8.2	5.85
VEC (e per Mo)	21.375	21.5	21.85
$\mu_0 H_{c2}$ (T) at $T = 2$ K	7.45	6.5	1.9
$2\Delta(0)/(k_BT_c)$	4.4	4.5	4.1
γ_N (mJ mol ⁻¹ K ⁻²)	99	67	39
γ_{bare} (mJ mol ⁻¹ K ⁻²)	52.7	31.1 ^t /39.1 ^m	20.0
λ_{ep}	0.9	0.84	0.95

parameter was observed [7].

The Mo₆Ga₃₁ superconductor with $T_c = 8$ K attracts interest as a possible candidate for multigap superconductivity. Physical properties of Mo₆Ga₃₁ are scarcely characterized in the literature: available information is based on the measurements carried out on the MoGa₄ sample, which nominal composition does not correspond to the actual stoichiometry of the compound. Moreover, the exact elemental and phase composition were not reported [3]. The measurements revealed superconductivity of the sample below $T_c = 8$ K in zero magnetic field with the upper critical field of $\mu_0 H_{c2} = 7.4$ T extrapolated to zero temperature [3].

Crystal structure of Mo_6Ga_{31} was probed in two independent studies. In the original investigation, monoclinic crystal structure in the $P2_1/c$ space group was reported [11]. However, single crystals, which adopt triclinic crystal structure, the P-1 space group, were also obtained under different synthetic conditions [12]. Both structures of Mo_6Ga_{31} , monoclinic and triclinic, are based on the same building unit, which is shown in Fig. 1 (a). The main building unit consists of Mo-embedded $Mo@Ga_{10}$ clusters and Ga-centered $Ga@Ga_{12}$ cuboctahedra. Twelve $Mo@Ga_{10}$ clusters form a distorted rectangular superprism, $\{Mo_{12}Ga_{62}\}$, where each $Mo@Ga_{10}$ cluster shares its triangular faces with the $Ga@Ga_{12}$ cuboctahedron,

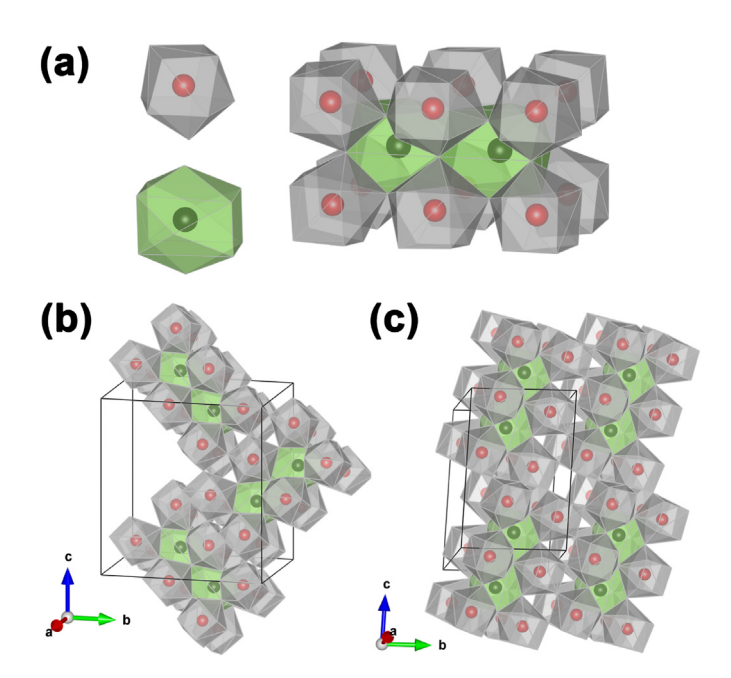


Fig. 1. (a) The main building unit of the Mo_6Ga_{31} crystal structure composed of $Mo@Ga_{10}$ polyhedra (gray) and $Ga@Ga_{12}$ cuboctahedra (green). The arrangement of building units in the monoclinic (b) and triclinic (c) modifications is shown in the bottom part of figure. (For interpretation of the references to colour in this figure legend, the reader is referred to the Web version of this article.)

and two adjacent Ga@Ga₁₂ cuboctahedra have a common rectangular face. In the monoclinic and triclinic structures, these building units connected by corners are perpendicular or codirectional to each other, respectively (Fig. 1(b and c)).

Herein, we thoroughly characterize the Mo_6Ga_{31} endohedral cluster superconductor by reporting its synthesis, crystal and electronic structure, and physical properties. We investigate the superconducting state of Mo_6Ga_{31} in order to measure the electron-phonon coupling, and analyze how it correlates with the critical temperature, density of states at the Fermi level, and valence electron count — the parameters that govern properties of the endohedral cluster superconductors.

2. Experimental details

MoGa $_{31}$ was synthesized using the standard ampule technique. The stoichiometric mixture of Mo (4N, powder) and Ga (5N, pieces) was placed inside a quartz ampule, which was evacuated to the residual pressure of 5×10^{-3} mbar and flame-sealed. To obtain a polycrystalline specimen of Mo $_6$ Ga $_{31}$, the ampule was annealed in a programmable furnace at 700 °C for 14 days with one intermediate grinding. The resulting black powder, which contains Mo $_6$ Ga $_{31}$ with no admixture of other compounds, was used for thermodynamic and electrical transport measurements. Single crystals of Mo $_6$ Ga $_{31}$ suitable for structural studies were selected from the specimens prepared under different synthetic conditions employing crystal growth from the high-temperature melt (see Section 3.1 for details).

High-resolution powder X-ray diffraction (HRPXRD) measurements were performed at the ID22 beam line ($\lambda=0.35451(1)$ Å, $2\theta_{max}=28$ °) of the European Synchrotron Radiation Facility (ESRF, Grenoble, France). Measurements were conducted at room temperature and at elevated temperatures using a hot-air blower on a sample enclosed in a fused silica capillary with a diameter of 0.3 mm. Le Bail fittings of the HRPXRD data were performed using the Jana2006 program [13]. HRPXRD patterns collected at elevated temperatures are presented in the Supporting Information. Polycrystalline specimen of Mo₆Ga₃₁ was studied by differential scanning calorimetry (DSC) using a STA 409 PC Luxx thermal analyzer (Netzsch). Measurements were performed in high-purity Ar atmosphere at temperatures between 30 °C and 600 °C with the heating/cooling rate of 10 °C/min, and the results are presented in the Supporting Information.

Three-dimensional electron diffraction (3D ED) patterns were collected on a Themis Z transmission electron microscope operated at 300 kV employing the InsteaDMatic script [14] for data acquisition. In a typical experiment, a crystal is continuously rotated while ED frames are collected over the tilt range of $\pm 50\,^\circ$ with the rotation speed of 0.43°/s. The exposure time of 0.3 s was used in the experiments. 3D ED patterns were visualized by the REDp program [15]. The collected 3D ED patterns and the corresponding energy-dispersive X-ray (EDX) specta are presented in the Supporting Information.

Single-crystal X-ray diffraction experiments were perfomed on a Bruker D8 Venture diffractometer (Mo X-ray source, graphite monochromator, $\lambda=0.71073$ Å, T=100K) equipped with a Photon 100 CMOS detector. For the absorption correction, the multi-scan routine was employed. The crystal structures were determined by the charge-flipping algorithm using the Superflip program [16], and refiend against $|F^2|$ using the SHELXL-2018 [17] and Jana2006 programs [13]. The atomic coordinates were standardized using the STRUCTURE TIDY program [18] as implemented in the VESTA software [19], which was also used for visualization of crystal structures.

Electronic structure calculations were performed within the framework of density functional theory using the full-potential

local-orbital minimum-basis band-structure code FPLO (version 14.00-47) [20]. The experimental structural data based on single-crystal XRD measurements were used in calculations. In the scalar relativistic regime, local density aproximation was used to treat the exchange and correlation energy [21]. Integrations were performed by the improved tetrahedron method [22] on a grid of $12 \times 12 \times 12$ k-points in the first Brillouin zone.

Electrical resistivity was measured by the standard four-probe technique using the AC transport option of a Physical Property Measurement System (PPMS, Quantum Design) at temperatures between 2 K and 300 K in magnetic fields from 0 T to 10 T. For measurements, a rectangular-shaped pellet with typical dimensions of $8 \times 3 \times 1$ mm³ was prepared by pressing the polycrystalline specimen at the external pressure of 4 kbar at room temperature. Cu wires with the diameter of 100 µm were attached to the pellet using silver-containing epoxy resin. Magnetization measurements were conducted on a Magnetic Properties Measurement System (MPMS 3 SQUID, Quantum Design) in the zerofield-cooling (zfc) and field-cooling (fc) conditions in the temperature range of 1.8-15 K in the magnetic field of 5 Oe. Also, magnetization was measured in the zfc conditions at various fixed temperatures between 2 K and 8 K by sweeping magnetic field from 0 T to 14 T using the VSM option of PPMS. Heat capacity was measured using a relaxation-type calorimeter (HC option of PPMS, Quantum Design) at temperatures between 1.8 K and 20 K in magnetic fields from 0 T to 10 T.

3. Results and discussion

3.1. Synthesis and crystal structure

Although two crystallographic modifications of Mo₆Ga₃₁ were reported, it is unclear, at which experimental conditions they can be obtained separately. Information on synthesis of the monoclinic Mo₆Ga₃₁ is missing in the original study [11], while single crystals of the triclinic Mo₆Ga₃₁ were obtained from the MoGa₉Si sample, in which the Mo₆Ga₃₁ phase was a side product [12]. We systematically studied synthetic conditions, at which single crystals of Mo₆Ga₃₁ can be obtained. The use of excess of Ga metal leads to crystallization of the Mo₈Ga₄₁ phase as the only product. Therefore, we performed syntheses of samples with the stoichiometric composition, while controlling the annealing temperature and the cooling rate. The annealing at 700 °C yields polycrystalline Mo₆Ga₃₁, whereas single crystals can be obtained by increasing the annealing temperature up to 1000 °C. Single crystals of the monoclinic Mo₆Ga₃₁ were selected from the sample, which was allowed to cool down to room temperature in the shut-off furnace (fast cooling). Single crystals adopting the triclinic structure were found in the sample, which was cooled at the rate of 4 °C/h (slow cooling). In both cases, tiny submillimeter-size single crystals were isolated. The bulk sample synthesized at 700 °C contains solely polycrystalline Mo₆Ga₃₁.

Single crystals selected from the samples were studied by single-crystal X-ray diffraction. Tables S1–S3 of the Supporting Information summarize the results, which are in good agreement with the previous reports [11,12], confirming the formation of two crystallographic modifications of Mo₆Ga₃₁. We should note the outstanding complexity of the crystal structures: the monoclinic structure contains 38 crystallographic sites [V = 2566.78(3) Å³, Z = 4, 148 atoms in the primitive cell], while there are 39 sites in the triclinic structure [V = 1282.75(2) Å³, Z = 2, 74 atoms in the primitive cell]. Given this complexity, it is natural to assume the formation of various types of defects in a polycrystalline specimen.

Room-temperature HRPXRD pattern of polycrystalline Mo_6Ga_{31} is presented in Fig. 2. The pattern confirms the absence of other

phases, such as Mo₈Ga₄₁, Mo₃Ga, elemental Mo or Ga. However, all peaks show significant broadening that could be ascribed to defects within the monoclinic phase or to symmetry lowering toward the triclinic structure. Indeed, Le Bail decomposition returned similar profile R factors of $R_p=6.3$, $R_{wp}=9.2$, and GOF=2.1 for the monoclinic unit cell, and $R_p = 6.4$, $R_{wp} = 9.3$, and GOF = 2.2 for the triclinic one. The refinement of two polymorphs simultaneously present in the sample is possible only with fixed volume fraction for each phase. Thus, this refinement gives no quantitative estimate of the polymorph ratio in the mixture. Upon heating up to 700 °C, the HRPXRD pattern remains qualitatively the same, while reflections shift due to the monotonous increase of the lattice parameters. Both temperature-dependent HRPXRD and complementary DSC experiments show no hints for a transformation between the triclinic and monoclinic polymorphs of Mo₆Ga₃₁ (see Supporting Information).

To gain insight into the local structure of polycrystalline Mo₆Ga₃₁, three-dimensional electron diffraction was employed providing 3D structural information from nm-size crystallites. 3D ED data were collected on crystallites with the lateral size of <500 \times 500 nm² in order to minimize the contribution from intergrowth and twinning. While testing the lattice type, two types of diffraction patterns with different unit cells were revealed corresponding to the monoclinic and triclinic modifications of Mo₆Ga₃₁. Both polymorphs were observed with similar probabilities on different crystallites. However, volume fractions of the monoclinic and triclinic polymorphs cannot be estimated from these data, because transmission electron microscopy is essentially a local-probe method. Unit cell determination by the REDp program [15,23] yields a = 9.37(4), b = 16.18(6), c = 16.48(1)Å, and $\beta = 94.7(1)^{\circ}$ for the monoclinic Mo₆Ga₃₁, and a = 9.37(5), b =9.47(3), c = 14.25(2)Å, $\alpha = 85.6(2)$, $\beta = 81.1(1)$, and $\gamma = 85.7(1)$ ° for the triclinic modification. Typical 3D ED patterns of the triclinic structure are shown in Fig. 3. The unit cell parameters are in good agreement with the single-crystal XRD results within the accuracy of the 3D ED method. EDX spectroscopy does not reveal any difference in the chemical composition of the studied crystallites (see Supporting Information). Based on the HRPXRD, DSC, and 3D ED studies, we conclude that both modifications of Mo₆Ga₃₁ are

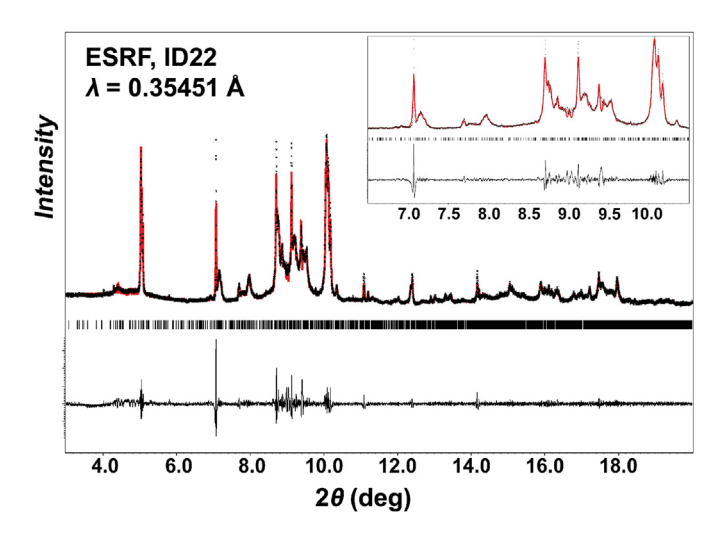


Fig. 2. Experimental (black points) and calculated (red line) high-resolution powder X-ray diffraction patterns of Mo_6Ga_{31} at room temperature. Positions of peaks are given by black ticks, and the difference curve is shown by the black line in the bottom part of figure. The inset shows a closer view of the low-angle diffraction peaks. (For interpretation of the references to colour in this figure legend, the reader is referred to the Web version of this article.)

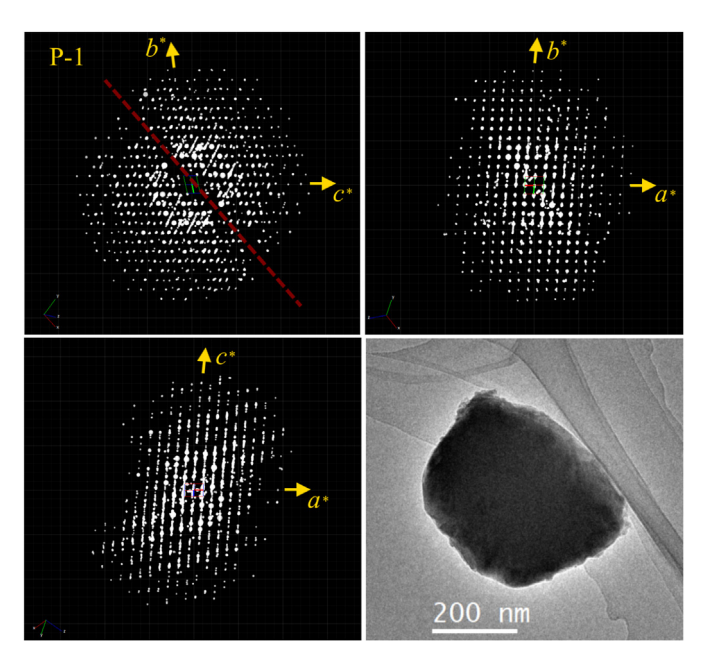


Fig. 3. Experimental 3D ED patterns of the triclinic Mo_6Ga_{31} , and the corresponding image of crystallite. Red dashed line shows the position of rotation axis towards the reciprocal space of the sample. (For interpretation of the references to colour in this figure legend, the reader is referred to the Web version of this article.)

inherently present in the bulk sample.

3.2. Electronic structure

Using the structural parameters obtained from the single-crystal XRD data, we calculated electronic structure of Mo_6Ga_{31} . The triclinic and monoclinic modifications possess qualitatively the same density of states (DOS), which is shown in Fig. 4. At low energies between -12 eV and -4 eV, mixing of the Ga 4s and 4p states is observed with a small contribution of the Mo 4d states. At higher energies between -4 eV and 4 eV, the Ga 4p and Mo 4d states contribute to the total DOS forming the peak substructure. The

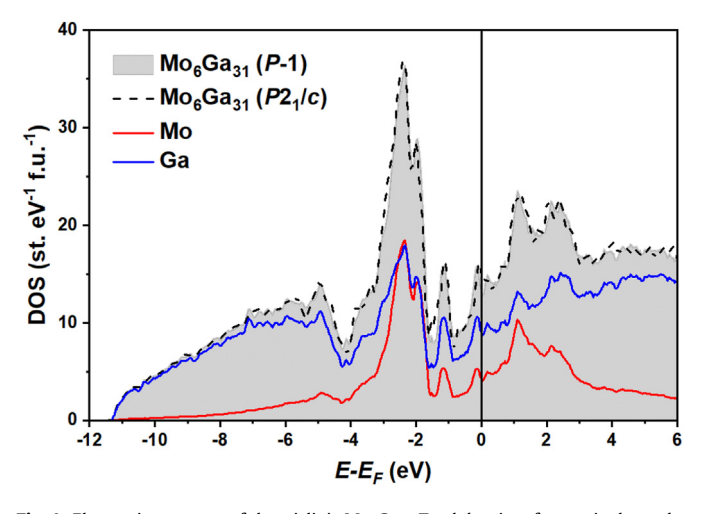


Fig. 4. Electronic structure of the triclinic Mo_6Ga_{31} . Total density of states is shown by the shaded area, the Mo and Ga contributions — by the solid red and blue lines, respectively. The density of states of the monoclinic structure is shown by the dashed line. The position of the Fermi level is indicated by the solid black line. (For interpretation of the references to colour in this figure legend, the reader is referred to the Web version of this article.)

Fermi level is located at the peak yielding a high value of DOS at E =E_F. The calculated electronic structure of Mo₆Ga₃₁ is similar to that of the Mo₈Ga₄₁ [6,9], Mo₄Ga_{21-x- δ}Sn_x [4], and Mo₇Ga_{52-x}Zn_x [24] endohedral cluster compounds, which also possess high DOS at E_F . For Mo₆Ga₃₁, we find $N(E_F) = 13$ st. eV⁻¹ f.u.⁻¹ for the triclinic structure and 17 st. eV⁻¹ f.u.⁻¹ for the monoclinic one. These values vield the bare Sommerfeld coefficients of 31 mJ mol⁻¹ K⁻² and $39 \text{ mJ} \text{ mol}^{-1} \text{ K}^{-2}$, respectively. For the reported endohedral cluster superconductors, the value of the density of states at the Fermi level correlates well with the observed critical temperature [1,4]. Given the high DOS at $E = E_F$ calculated for Mo₆Ga₃₁, which is comparable with those of the Mo₈Ga₄₁ and Mo₄Ga_{21-x- δ}Sn_x superconductors, we expect superconducting behavior for both crystallographic modifications of Mo₆Ga₃₁. However, triclinic and monoclinic Mo₆Ga₃₁ should possess slightly different super conducting-state parameters, including the critical temperature, T_c , and full superconducting gap, $2\Delta(0)/(k_BT_c)$. Our HRPXRD and 3D ED studies show that the triclinic and monoclinic structures are in the strong contact with each other in the bulk specimen. Due to the proximity effect [25], the superconducting carriers travel coherently between two superconducting phases, and thus, intermediate superconducting parameters should be observed, corresponding effectively to one superconducting phase.

3.3. Physical properties

Electrical resistivity of Mo_6Ga_{31} follows metallic behavior at elevated temperatures (Fig. 5). However, the $\rho(T)$ dependence is extremely flat between 10 K and 300 K, and shows the saturation behavior with increasing temperature. The small residual-resistance-ratio of 1.2 can be paralleled to the peak broadening observed in HRPXRD and caused by the coexisting domains of the monoclinic and triclinic phases. At low temperatures, superconducting transition is observed with the low-temperature drop of resistivity occurring between the onset temperature of 8.2 K and the final temperature of 7.8 K in zero magnetic field. The increase of magnetic field shifts the transition to lower temperatures, and finally, no indications of superconductivity are observed at temperatures above 1.8 K in the magnetic field of $\mu_0H=10$ T.

The bulk nature of superconductivity is confirmed by thermodynamic measurements (Fig. 6). Dimensionless volume magnetic susceptibility shows diamagnetic shift due to the Meissner effect below the critical temperature of $T_c = 8.2$ K in 5 Oe magnetic field. The zfc signal of -0.94 at the lowest measured temperature

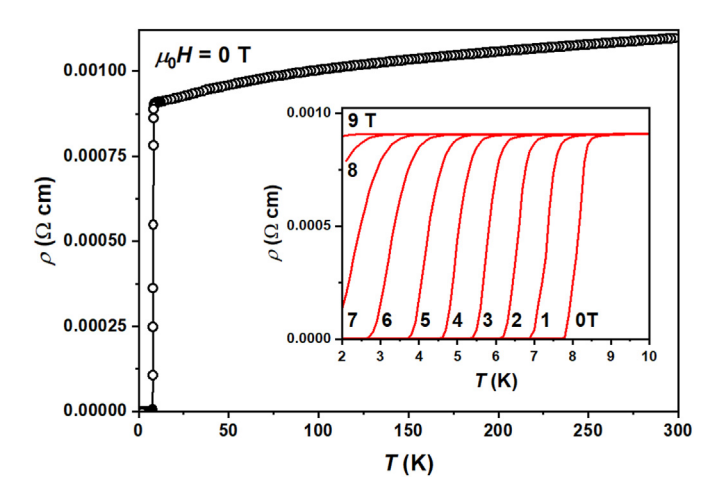


Fig. 5. Electrical resistivity of Mo_6Ga_{31} in zero magnetic field. The inset shows the data at low temperatures in magnetic fields between 0 T and 9 T.

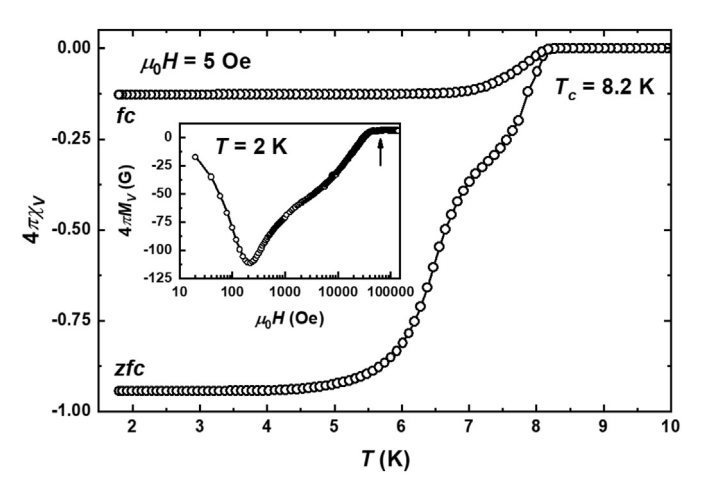


Fig. 6. Dimensionless volume magnetic susceptibility of Mo_6Ga_{31} measured in 5 Oe magnetic field in the zfc and fc conditions. The inset shows volume magnetization measured in the zfc conditions at T=2 K. The arrow indicates the transition to the normal state.

indicates large volume fraction of the superconducting phase. The transition is broadening with temperature and shows a pronounced shoulder at ~ 7 K, which is presumably caused by the inhomogeneities of the specimen, including point and extended defects, as well as domains of the triclinic and monoclinic phases. The difference in transition temperatures of monoclinic and triclinic Mo₆Ga₃₁ may cause such a shoulder. Volume magnetization, which is shown in the inset of Fig. 6, is characteristic of type-II superconductors. Note that the logarithmic scale is used in figure to represent the magnetic fields. In low magnetic fields, $4\pi M_V$ follows the linear behavior versus $\mu_0 H$ below the lower critical field of $\mu_0 H_{c1} = 700e$ at T = 2 K. With the increase of magnetic field, the normal state is achieved above the upper critical field of $\mu_0 H_{c2} =$ 6.5 T at T=2 K. Between $\mu_0 H_{c1}$ and $\mu_0 H_{c2}$, the volume magnetization exhibits intricate nonmonotonic behavior, which also evidences the presence of inhomogeneities in the specimen.

The specific heat of Mo_6Ga_{31} exhibits the superconducting anomaly located at $T_c=8.2$ K in zero magnetic field in good agreement with the resistivity and magnetization measurements. The increase of the magnetic field shifts the transition to lower temperatures, which simultaneously becomes smoothed (Fig. 7). The temperature sweeps of resistivity and heat capacity measured in various magnetic fields, as well as the field sweeps of

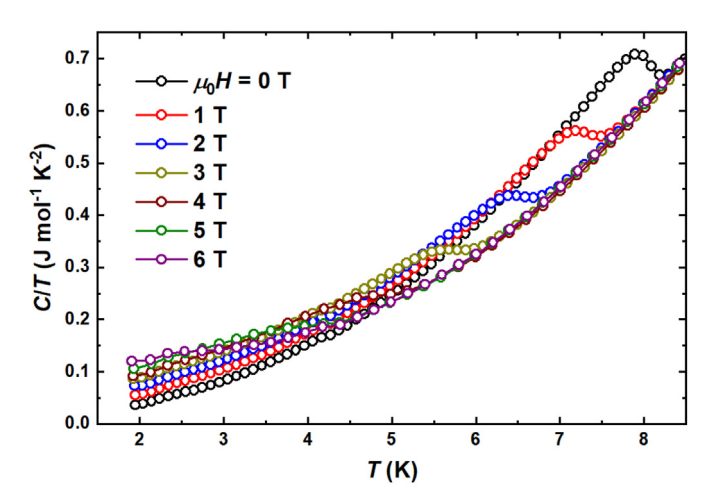


Fig. 7. Specific heat of Mo₆Ga₃₁ in various magnetic fields.

magnetization at constant temperatures were used to extract the upper critical field of Mo₆Ga₃₁ as a function of temperature (Fig. 8). The $\mu_0 H_{c2}(T)$ values, which correspond to the onset temperature of the resistivity drop, are larger than those from the magnetization and heat capacity measurements. From the other hand, the temperatures, at which zero resistance is achieved, yields $\mu_0 H_{c2}(T)$. which are closer to the thermodynamic measurements. The magnetization and heat-capacity derived $\mu_0H_{c2}(T)$ values are in good agreement with each other. Above these values, the bulk of the sample is in the normal state. Interpolation of the $\mu_0 H_{c2}(T)$ values by the second-order polynomial yields $\mu_0 H_{c2}(0) =$ 7.8T at zero temperature, which is in good agreement with the previous report [3]. The $\mu_0 H_{c2}(0)$ value corresponds to the Ginzburg-Landau coherence length of $\xi=6.5 \,\mathrm{nm}$ as calculated from the equation $\mu_0 H_{c2}(0)=\frac{\Phi_0}{2\pi \xi_{cL}^2}$, where $\Phi_0=h/2e$ is the flux quantum. At temperatures above 6 K, $\mu_0 H_{c2}(T)$ is linear with the slope of $\omega = -1.2T \text{ K}^{-1}$. According to the Werthamer-Helfand-Honenberg (WHH) model, the upper critical field can be calculated as $\mu_0 H_{c2}(0) = -0.693 \omega T_c = 6.8$ T, which is smaller than the extrapolated value of $\mu_0 H_{c2}(0) = 7.8$ T. This enhancement of the upper critical field may be due to strong electron-phonon coupling.

To gain insight into the electron-phonon coupling in the superconducting state of Mo₆Ga₃₁, the specific heat data were analyzed. Fig. 9 shows the specific heat in superconducting ($\mu_0H=0$ T) and normal states ($\mu_0H=10$ T). The normal-state specific heat can be fitted using the equation $C(T)=\gamma T+\beta T^3+\delta T^5$ in the temperature range of 1.8–10 K yielding $\gamma=67(1)$ mJ mol⁻¹ K⁻², $\beta=5.6(2)$ mJ mol⁻¹ K⁻⁴, and $\delta=40(3)\mu$ J mol⁻¹ K⁻⁶ (solid red line in Fig. 9). The value of β corresponds to the Debye temperature of $\Theta_D=234(2)$ K,

as calculated from
$$\Theta_D = \left(\frac{12\pi^4Rn}{5\beta}\right)^{1/3} = [(1.944 \times 10^6)n/\beta]^{1/3}$$
,

where R is the molar gas constant, n=37 is the number of atoms per formula unit, and the equality on the far right-hand side is Θ_D in [K] and β in [m] mol $^{-1}$ K $^{-4}$]. The electronic specific heat, which is shown in the inset of Fig. 9, was calculated as $\Delta C_e/T = \Delta C/T(0T) - \Delta C/T(10T)$ and analyzed within the BCS-derived α -model [26,27]. The fitting yields the full superconducting gap of $2\Delta(0)/(k_BT_c)=4.5$, the normalized specific heat jump of $\Delta C_e/(\gamma_N T_c)=2.3$ at $T=T_c$, and the normal-state Sommerfeld coefficient of $\gamma_N=67$ mJ mol $^{-1}$ K $^{-2}$. Remarkably, the transition is smoothed with temperature, which is seen as the difference between the experimental data (black open circles in the inset of Fig. 9) and the calculated specific heat (solid red

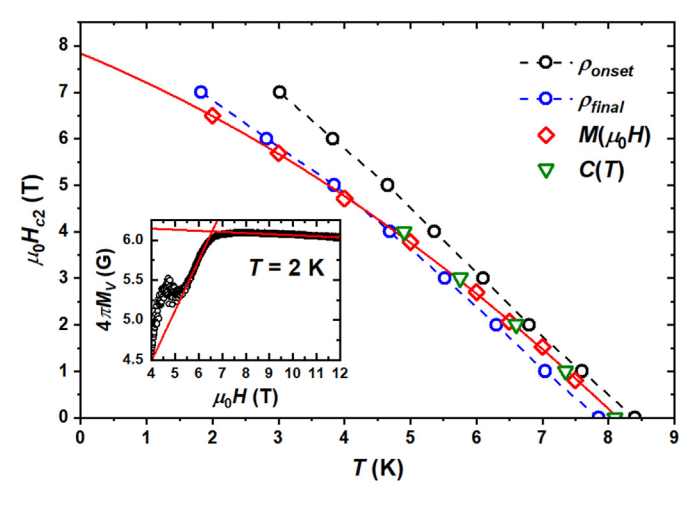


Fig. 8. Upper critical field of Mo_6Ga_{31} . The inset shows a linear construction of the volume magnetization curve used for the determination of the upper critical field.

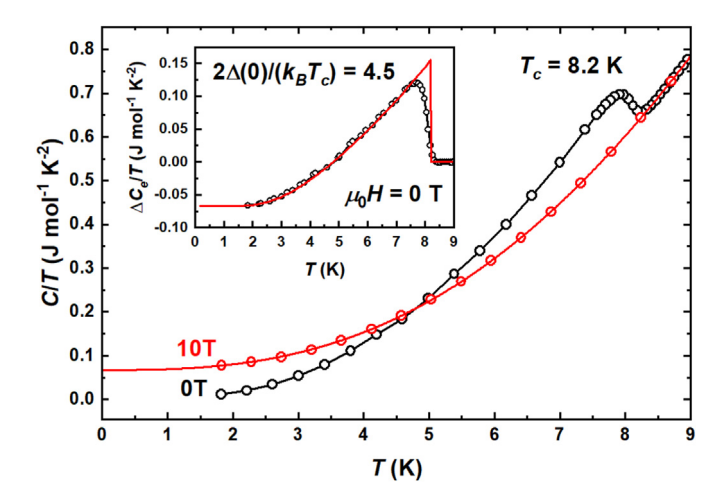


Fig. 9. Specific heat of Mo_6Ga_{31} measured in 0 T and 10 T magnetic fields. The solid red line is a fit of the normal-state heat capacity (see in the text) The inset shows the electronic contribution to the total heat capacity in zero magnetic field. The red line is a fit according to the α -model. (For interpretation of the references to colour in this figure legend, the reader is referred to the Web version of this article.)

line) in the vicinity of the critical temperature, which may be caused by the coexisting domains of the monoclinic and triclinic phases. Both the enhanced value of $\Delta C_e/(\gamma_N T_c)=2.3$, which is larger than the weak-coupling BCS limit of $\Delta C_e/(\gamma_N T_c)=1.43$, and the large value of $\alpha=2.25$ point to the strong electron-phonon coupling in the superconducting state. The electron-phonon coupling constant λ_{ep} can be estimated using the McMillan's formula for a strongly-coupled single-gap superconductor [28]:

$$\lambda_{ep} = \frac{1.04 + \mu^* \ln\left(\frac{\Theta_D}{1.45T_c}\right)}{(1 - 0.62\mu^*) \ln\left(\frac{\Theta_D}{1.45T_c}\right) - 1.04},\tag{1}$$

where μ^* is the Coulomb pseudopotential. $\mu^*=0.13$, $T_c=8.2$ K, and $\Theta_D=234$ K yield $\lambda_{ep}=0.84$ implying the strong electron-phonon coupling in the superconducting state. Thus, Mo₆Ga₃₁ is a strongly-coupled superconductor similar to the Mo₈Ga₄₁ and Mo₄Ga_{21-x- δ}Sn_x related compounds [4,6,7].

In Table 1, we compare normal- and superconducting-state properties of Mo₈Ga₄₁, Mo₆Ga₃₁, and Mo₄Ga_{21-x- δ}Sn_x. The observed T_c values follow the trend of decreasing the critical temperature with increasing the valence electron count (VEC), which was proposed for endohedral cluster superconductors [1]. Moreover, it is obvious that the critical temperature correlates well with the value of DOS at $E=E_F$: both γ_N and γ_{bare} decrease with decreasing T_c . At the same time, the values of full superconducting gap, $2\Delta(0)/(k_BT_c)$, and electron-phonon coupling constant, λ_{ep} , are practically the same in the series indicating that the strength of the electron-phonon coupling in the superconducting state has no significant impact on the critical temperature.

4. Conclusions

In the paper, synthesis, structural characteristics, computational electronic structure, and physical properties of the Mo_6Ga_{31} superconductor are reported. The bulk type-II superconductivity is observed below the critical temperature of 8.2 K in zero magnetic field, and below the upper critical field of 7.8 T extrapolated to zero temperature. Remarkably, the superconducting state is in the strong-coupling regime with the large ratio of $2\Delta/(k_BT_c)=4.5$.

CRediT authorship contribution statement

Valeriy Yu. Verchenko: Writing - original draft, Methodology, Data curation, Formal analysis. Alexander O. Zubtsovskii: Data curation. Alexander A. Tsirlin: Methodology. Zheng Wei: Data curation. Maria Roslova: Data curation, Formal analysis. Evgeny V. Dikarev: Conceptualization, Project administration. Andrei V. Shevelkov: Conceptualization, Project administration.

Declaration of competing interest

The authors declare that they have no known competing financial interests or personal relationships that could have appeared to influence the work reported in this paper.

Acknowledgements

The authors acknowledge the European Synchrotron Radiation Facility for granting the beam time and thank Dr. Wilson Mogodi for his help during the high-resolution PXRD experiments. The work was supported by the Russian Science Foundation, grant no. 17-13-01033. V.Yu.V. acknowledges the financial support from the Mobilitas program of the European Science Foundation, grant no. MOBJD449. A.A.T. appreciates financial support by the Federal Ministry for Education and Research under the Sofja Kovalevskaya Award of the Alexander von Humboldt Foundation. Z.W. and E.V.D. thank the National Science Foundation for supporting structural studies under grant no. CHE-1955585.

There are no conflicts to declare.

Appendix A. Supplementary data

Supplementary data to this article can be found online at https://doi.org/10.1016/j.jallcom.2020.156400.

References

- [1] W. Xie, H. Luo, B.F. Phelan, T. Klimczuk, F.A. Cevallos, R.J. Cava, Endohedral gallide cluster superconductors and superconductivity in ReGa₅, Proc. Natl. Acad. Sci. U.S.A. 112 (51) (2015) E7048–E7054, https://doi.org/10.1073/ pnas.1522191112.
- [2] A. Bezinge, K. Yvon, M. Decroux, J. Muller, On the existence of binary Mo₈Ga₄₁ and its properties, J. Less Common. Met. 99 (2) (1984) L27–L31, https://doi.org/10.1016/0022-5088(84)90237-6.
- [3] O. Fischer, Properties of high field superconductors, containing localized magnetic moments, Helv. Phys. Acta 45 (3) (1972) 331–397, https://doi.org/ 10.5169/seals-114388.
- [4] V.Y. Verchenko, A.O. Zubtsovskii, Z. Wei, A.A. Tsirlin, M. Marcin, A.V. Sobolev, I.A. Presniakov, E.V. Dikarev, A.V. Shevelkov, Endohedral cluster superconductors in the Mo—Ga—Sn system explored by the joint flux technique, Inorg. Chem. 58 (2019) 15552–15561, https://doi.org/10.1021/acs.inorgchem. 9h02598

- [5] T. Shibayama, M. Nohara, H.A. Katori, Y. Okamoto, Z. Hiroi, H. Takagi, Super-conductivity in Rh₂Ga₉ and Ir₂Ga₉ without inversion symmetry, J. Phys. Soc. Jpn. 76 (2007), 073708, https://doi.org/10.1143/JPSJ.76.073708.
- [6] V.Y. Verchenko, A.A. Tsirlin, A.O. Zubtsovskiy, A.V. Shevelkov, Strong electronphonon coupling in the intermetallic superconductor Mo₈Ga₄₁, Phys. Rev. B 93 (2016), 064501, https://doi.org/10.1103/PhysRevB.93.064501.
- [7] M. Marcin, J. Kačmarčík, Z. Pribulová, M. Kopčík, P. Szabó, O. Šofranko, T. Samuely, V. Vaňo, C. Marcenat, V.Y. Verchenko, A.V. Shevelkov, P. Samuely, Single-gap superconductivity in Mo₈Ga₄₁, Sci. Rep. 9 (2019) 13552, https://doi.org/10.1038/s41598-019-49846-y.
- [8] V.Y. Verchenko, R. Khasanov, Z. Guguchia, A.A. Tsirlin, A.V. Shevelkov, Two-gap superconductivity in Mo₈Ga₄₁ and its evolution upon vanadium substitution, Phys. Rev. B 96 (2017) 134504, https://doi.org/10.1103/PhysRevB 96 134504
- [9] A. Sirohi, S. Saha, P. Neha, S. Das, S. Patnaik, T. Das, G. Sheet, Multiband superconductivity in Mo₈Ga₄₁ driven by a site-selective mechanism, Phys. Rev. B 99 (5) (2019), 054503, https://doi.org/10.1103/PhysRevB.99.054503.
- [10] Z. Hu, D. Graf, Y. Liu, C. Petrovic, Three-dimensional Fermi surface and small effective masses in Mo₈Ga₄₁, Appl. Phys. Lett. 116 (2020) 202601, https:// doi.org/10.1063/5.0005177.
- [11] K. Yvon, The crystal structure of Mo₆Ga₃₁, a hypersymmetrical structure solved by direct methods, Acta Crystallogr. B 30 (4) (1974) 853–861, https:// doi.org/10.1107/S0567740874010958.
- [12] R. Lux, Dissertation: Intermetallische Verbindungen mit hochschmelzenden Übergangsmetallen und niedrigschmelzenden Metallen, University of Freiburg, Freiburg, Germany, 2004.
- [13] V. Petříček, M. Dušek, L. Palatinus, Crystallographic computing system JANA2006: general features, Z. Kristallogr. 229 (5) (2014) 345, https://doi.org/ 10.1515/zkri-2014-1737.
- [14] M. Roslova, S. Smeets, B. Wang, T. Thersleff, H. Xu, X. Zou, Towards Cross-Platform Automated Rotation Electron Diffraction, 2019 arXiv:arXiv: 1911.09393
- [15] W. Wan, J. Sun, J. Su, S. Hovmöller, X. Zou, Three-dimensional rotation electron diffraction: software *RED* for automated data collection and data processing, J. Appl. Crystallogr. 46 (2013) 1863–1873, https://doi.org/10.1107/S0021889813027714.
- [16] L. Palatinus, G. Chapius, Superflip a computer program for the solution of

- crystal structures by charge flipping in arbitrary dimensions, J. Appl. Crystallogr, 40 (4) (2007) 786–790, https://doi.org/10.1107/S0021889807029238.
- [17] G.M. Sheldrick, Crystal structure refinement with SHELXL, Acta Crystallogr. C: Struct. Chem. C71 (2015) 3–8, https://doi.org/10.1107/S2053229614024218.
- [18] L.M. Gelato, E. Parthé, Structure TIDY a computer program to standardize crystal structure data, J. Appl. Crystallogr. 20 (1987) 139–143, https://doi.org/ 10.1107/S0021889887086965.
- [19] K. Momma, F. Izumi, VESTA 3 for three-dimensional visualization of crystal, volumetric and morphology data, J. Appl. Crystallogr. 44 (6) (2011) 1272–1276, https://doi.org/10.1107/S0021889811038970.
- [20] K. Koepernik, H. Eschrig, Full-potential nonorthogonal local-orbital minimumbasis band-structure scheme, Phys. Rev. B 59 (1999) 1743, https://doi.org/ 10.1103/PhysRevB.59.1743.
- [21] J.P. Perdew, Y. Wang, Accurate and simple analytic representation of the electron-gas correlation energy, Phys. Rev. B 45 (1992) 13244, https://doi.org/ 10.1103/PhysRevB.45.13244.
- [22] P.E. Blöchl, O. Jepsen, O.K. Andersen, Improved tetrahedron method for brillouin-zone integrations, Phys. Rev. B 49 (1994) 16223, https://doi.org/ 10.1103/PhysRevB 49.16223
- [23] W. Kabsch, Xds, Acta Crystallogr. D 66 (2010) 125–132, https://doi.org/ 10.1107/S0907444909047337.
- [24] V.Y. Verchenko, A.O. Zubtsovskii, Z. Wei, A.A. Tsirlin, E.V. Dikarev, A.V. Shevelkov, From endohedral cluster superconductors to approximant phases: synthesis, crystal and electronic structure, and physical properties of Mo₈Ga^{41-X}Zn_x and Mo₇Ga^{52-X}Zn_x, Dalton Trans. 48 (2019) 7853, https:// doi.org/10.1039/c8dt04982c.
- [25] C.P. Poole, Handbook of Superconductivity, Academic Press, 525 B Street, Suite, San Diego, CA, 1900, 92101-4495, USA, 2000.
- [26] H. Padamsee, J.E. Neighbor, C.A. Shiffman, Quasiparticle phenomenology for thermodynamics of strong-coupling superconductors, J. Low Temp. Phys. 12 (1973) 387–411, https://doi.org/10.1007/BF00654872.
- [27] D.C. Johnston, Elaboration of the α-model derived from the BCS theory of superconductivity, Supercond. Sci. Technol. 26 (2013) 115011, https://doi.org/ 10.1088/0953-2048/26/11/115011.
- [28] W.L. McMillan, Transition temperature of strong-coupled superconductors, Phys. Rev. 167 (1968) 331–344, https://doi.org/10.1103/PhysRev.167.331.